Assessing Hydraulic Hysteresis Models to Characterize Unsaturated Flow Behavior under Drying and Wetting Conditions

Jie Liu[1]; Pan Chen[2]; and Wentao Li[3]

Abstract: A soil-water retention curve (SWRC) is one of the important constitutive laws for soil-water distribution and shear-strength assessment in unsaturated soil. A SWRC commonly shows the hysteretic behavior under drying and wetting conditions. Several mathematical models have been developed to describe hysteresis, including a model commonly presented in the literature and implemented into HYDRUS software. Recently, the authors developed a new hydraulic hysteresis model for which only one additional parameter was introduced to capture the effects of capillary and air-entrapment hysteresis. To confirm the capabilities of the two models in analyzing the unsaturated flow, the authors' model was implemented with a numerical code using the FORTRAN language. The numerical codes including the authors' model and the model in HYDRUS for hysteresis assessment were used to analyze the same transient unsaturated flow problems under drying and wetting conditions. By comparing the measured data to curves predicted by the two models, the results show that the hysteretic SWRC cannot be described correctly when the effects of hydraulic hysteresis are ignored under drying and wetting conditions. Moreover, the comparison between the results predicted by the two models shows that the authors' model gave a robust performance for capturing hydraulic hysteresis behavior in unsaturated flow. **DOI: 10.1061/(ASCE)GM.1943-5622.0001205.**

Author keywords: Unsaturated soil; Soil-water retention; Hydraulic hysteresis; Unsaturated flow; Finite element method.

Introduction

Hydraulic hysteresis, including the effects of capillary and air-entrapment hysteresis, commonly occurs in variably unsaturated soils under drying and wetting conditions [e.g., Khalili et al. (2008); Sun et al. (2010); Sheng and Zhou (2011); Lu et al. (2013); Dongmei et al. (2016); Pasha et al. (2017)]. Because of the nonuniform distribution of pore sizes in soils, the soil-water retention (SWR) behavior typically shows many differences under drying and wetting conditions; the behavior under these conditions is called *capillary hysteresis* [e.g., Poulovassilis (1970); Scott et al. (1983); Feng and Fredlund 1999]. Furthermore, pore air is usually be trapped in some pores when soil experiences a wetting process; because of this, a fully saturated state cannot be reached in soil even when the matric suction decreases to zero. The phenomenon of the air entrapped in unsaturated soils is generally called *air-entrapment hysteresis* [e.g., Bond and Collis-George (1981)]. However, one or two effects of the hydraulic hysteresis described in this paragraph were usually ignored in analyses of unsaturated flow problems. For example, the initial drying curve (IDC) was often used to describe SWR behavior under intermittent rain infiltration and water table fluctuation conditions [e.g., Baum et al. (2010); BeVille et al. (2010); Tami et al. (2004); Sun et al. (2016)]. Nevertheless, the significant influence of hydraulic hysteresis on unsaturated flow has been confirmed in the literature [e.g., Stonestrom and Rubin (1989); Seymour (2000); Likos et al. (2014); Chen and Wei (2016)] and mechanical behavior of unsaturated soils [e.g., Khoury and Miller (2012), Khoury et al. (2012); Liu and Muraleetharan (2012); Chen et al. (2013); Ma et al. (2016)]. Hence, the inclusion of the effect of hydraulic hysteresis is crucial in analyses of subsurface flow and transport processes [e.g., Pickens and Gillham (1980); Yang et al. (2012); Li et al. (2014)], and such effect must be considered in assessments of slope stability under rainfall infiltration conditions [e.g., Ebel et al. (2010); Chen et al. (2017)].

Some mathematical models have been developed and applied to describe the effect of hydraulic hysteresis on the SWR curve (SWRC) under drying and wetting conditions [e.g., Parker and Lenhard 1987; Pham et al. 2005; Khalili et al. 2008)]. In the early stages of SWR research, the domain model was widely used to characterize the capillary hysteresis of SWR behavior (Poulovassilis and Childs 1971; Mualem and Dagan 1975). Vachaud and Thony (1971) pointed out that the domain model was insufficient to describe the SWRC with capillary hysteresis, for which the drainage in all pores is independent. According to the hypothesis of similarity between the boundary and scanning curves, the scaling approach was used to describe the capillary hysteresis behavior of SWR [e.g., Parlange (1976); Scott et al. (1983); Kool and Parker (1987)]. However, the assumption of the capillary tube model was used, and the hysteresis of the contact angle was neglected in the scaling models [e.g., Kechavarzi et al. (2005)]. The scaling hysteresis model was often used to analyze the unsaturated flow problem

[1]Assistant Professor, State Key Laboratory of Geomechanics and Geotechnical Engineering, Institute of Rock and Soil Mechanics, Chinese Academy of Sciences, Wuhan, Hubei, 430071, P. R. China. Email: Liujie_whrsm@163.com

[2]Associate Professor, State Key Laboratory of Geomechanics and Geotechnical Engineering, Institute of Rock and Soil Mechanics, Chinese Academy of Sciences, Wuhan, Hubei, 430071, P. R. China (corresponding author). Email: pchen@whrsm.ac.cn

[3]Assistant Professor, State Key Laboratory of Geomechanics and Geotechnical Engineering, Institute of Rock and Soil Mechanics, Chinese Academy of Sciences, Wuhan, Hubei, 430071, P. R. China. Email: lwtdn@sina.com

Note. This manuscript was submitted on September 21, 2017; approved on February 2, 2018; published online on May 9, 2018. Discussion period open until October 9, 2018; separate discussions must be submitted for individual papers. This paper is part of the ***International Journal of Geomechanics***, © ASCE, ISSN 1532-3641.

under drying and wetting conditions [e.g., Kool and Parker (1987); Parker and Lenhard (1987)]. Furthermore, the model of Kool and Parker (1987) was implemented into HYDRUS software (Šimůnek et al. 2012). In addition, the hysteretic SWRC was simplified by two straight lines on behalf of the main boundary curves in the semilogarithmic scales [e.g., Wheeler et al. (2003); Khalili et al. (2008); Sun et al. (2007); Sheng and Zhou (2011)]. Although it was easily implemented into a numerical code, such a simplified method was not sufficient to describe any scanning drying or wetting curve [e.g., Huang et al. (2005)]. Recently, a new hydraulic hysteresis model was proposed that can capture the effects of capillary and air-entrapment hysteresis (Chen et al. 2015) on the basis of a model developed by Wei and Dewoolkar (2006). In addition to the initial drying and main wetting curves (MWCs), the model included only one additional parameter to describe the scanning SWRC when soil experiences drying and wetting conditions.

To validate the Chen et al. (2015) model effectively, the hysteresis model developed by Kool and Parker (1987), which was widely used and cited in the literature, was chosen as the reference. Although several advanced SWRC models have been developed to describe the capillary hysteresis behavior coupled with the hysteretic SWRC and soil deformation [e.g., Khalili et al. (2008); Sheng and Zhou (2011)], the deformation of soil is not the main concern of this paper.

First, to simulate the unsaturated flow problems and validate the capability of the model describing the hysteretic SWRC, the model of Chen et al. (2015) was used with a finite-element code. Then, to assess the differences of the two numerical models, the software HYDRUS, including the model of Kool and Parker (1987) and the proposed numerical model, were used to simulate the same unsaturated flow problem. Finally, the two numerical models were used to simulate hysteretic unsaturated flow. The advantages and disadvantages between the two numerical models with different hysteresis models were determined by comparing the simulated results to the measured data. Meanwhile, the importance of hydraulic hysteresis on unsaturated flow was explored in detail by comparing the results from considering and ignoring it.

Theoretical Formulas of Hysteresis Models

To describe the hydraulic hysteresis behavior of the SWRC, Kool and Parker (1987) developed a SWRC model using a scaling approach that was based on the similarity hypothesis. Chen et al. (2015) developed a hydraulic hysteresis model that included the effects of capillary and air-entrapment hysteresis on the basis of the Wei and Dewoolkar (2006) model. The mathematic descriptions for the two hysteresis models are given in brief in the remainder of this section.

Kool and Parker (1987) Model

The SWRC model developed by van Genuchten (1980) was used to describe the IDC and the MWC. The IDC is described as

$$S_e = \frac{\theta - \theta_r^d}{\theta_s^d - \theta_r^d} = \left[1 + \left(\alpha^d \psi^d\right)^{n^d}\right]^{-m^d} \tag{1}$$

The MWC is described as

$$S_e = \frac{\theta - \theta_r^w}{\theta_s^w - \theta_r^w} = \left[1 + \left(\alpha^w \psi\right)^{n^w}\right]^{-m^w} \tag{2}$$

where S_e = effective degree of saturation; ψ = soil suction (in kilopascals); θ = volumetric water content; θ_r^d and θ_r^w = residual volumetric water content for the IDC and MWC, respectively; θ_s^d = saturated volumetric water content and equals the porosity of soil, η_0; θ_s^w = volumetric water content for the MWC at zero soil suction; and α, m, and n = model parameters. The parameters α^d and n^d are obtained by fitting the measured initial drying data; α^w and n^w are obtained by fitting the measured main wetting data using the least-squares method; and m is determined by a common restriction, $m = 1 - 1/n$ (van Genuchten 1980).

Then, through use of the strategy developed by Scott et al. (1983), the water content on a drying scanning curve at soil suction ψ is scaled, as follows, from the IDC when the reversal point (θ_Δ, ψ_Δ) is given, [e.g., Šimůnek et al. (2012)]:

$$\theta(\psi) = \theta_r^{ds} + \beta\left[\theta^d(\psi) - \theta_r^d\right] \tag{3}$$

where $\theta^d(\psi)$ = volumetric water content on the IDC at soil suction, ψ; β = parameter related to the reversal point, $\beta = (\theta_\Delta - \theta_r^d)/\left[\theta^d(\psi) - \theta_r^d\right]$; θ_r^{ds} = residual volumetric water content for a drying scanning curve, $\theta_r^{ds} = \theta_s - \beta\left(\theta_s^d - \theta_r^d\right)$; and θ_s = volumetric water content for a scanning curve at zero soil suction, $\theta_s = \theta_s^d - \left(\theta_s^d - \theta_\Delta\right)/\left[1 + R\left(\theta_s^d - \theta_\Delta\right)\right]$, where $R = 1/\left(\theta_s^d - \theta_s^w\right) - 1/\left(\theta_s^d - \theta_r^d\right)$.

Similarly, the wetting scanning curve at soil suction, ψ, is scaled as follows from the MWC when the reversal point (θ_Δ, ψ_Δ) is given (e.g., Šimůnek et al. 2012):

$$\theta(\psi) = \theta_r^{ws} + \gamma\left[\theta^w(\psi) - \theta_r^w\right] \tag{4}$$

where θ_r^{ws} = residual volumetric water content for the wetting scanning curve, $\theta_r^{ws} = \theta_s - \gamma(\theta_s^w - \theta_r^w)$; $\theta^w(\psi)$ = volumetric water content on the MWC at the soil suction, ψ; and γ = parameter related to the reversal point, $\gamma = (\theta_\Delta - \theta^s)/\left[\theta^w(\psi) - \theta_s^w\right]$.

Some constraints are imposed on the hysteresis model to reduce the number of model parameters as follows:

$$\theta_r^d = \theta_r^w = \theta_r \tag{5a}$$

If the content of air entrapment is negligible, then another constraint is

$$\theta_s^d = \theta_s^w \tag{5b}$$

Moreover, the following constraint is needed to define a nonhysteretic conductivity function, $k(\theta)$:

$$n^d = n^w = n \tag{5c}$$

As explained by Kool and Parker (1987), the constraint in Eq. (5c) weakens the flexibility of the hysteresis model in characterizing SWR behavior, which was shown in the simulated results (as presented herein). The model for the hydraulic conductivity function, $k(\theta)$, developed by Mualem (1976), is described as

$$k(S_e) = k_{sat} S_e^{0.5}\left[1 - \left(1 - S_e^{1/m}\right)^m\right]^2 \tag{6}$$

where k_{sat} = saturated hydraulic conductivity.

Eight parameters (θ_s^d, θ_s^w, θ_r^d, θ_r^w, α^d, α^w, n^d, and n^w) were in the model of Kool and Parker (1987) for characterizing the hysteretic SWRC, including the effect of capillary and air-entrapment hysteresis. Under the constraints of Eqs. (5a) and (5c), six parameters (θ_s^d, θ_s^w, θ_r, α^d, α^w, and n) described the hydraulic hysteretic behavior, and five parameters (θ_s^d, θ_r, α^d, α^w, and n) were used to

determine the SWRC with only capillary hysteresis in the Kool and Parker (1987) model. The parameters θ_s^d, θ_r, α^d, and n were obtained by fitting the measured IDC using Eq. (1). The parameters θ_s^w and α^w were obtained by fitting the measured MWC using Eq. (2). The hysteresis model was implemented into the HYDRUS software [e.g., Šimůnek et al. (2012)].

Hydraulic Hysteresis Model Developed by Chen et al. (2015)

The hydraulic hysteresis model developed by Chen et al. (2015) is described simply herein. The boundary curves, namely IDC (A–B) and MWC (B–C), needed to be defined to describe the hysteretic loops (C′–D′–C′), as seen in Fig. 1(a).

For consistency, the SWRC model developed by van Genuchten (1980) was also used in this model to describe the IDC and MWC by Eqs. (1) and (2), respectively. The scanning curves within the boundary curves were determined by the model developed by Chen et al. (2015) as described in this paragraph. For a hysteretic loop, such as loop C–D–C, where current drying and wetting cycles are located, and the boundaries of loop C–B–C are specified, any scanning curve included in the current loop, from the initial Point D, can be described by

$$\Delta S = \Delta\psi / K_p\left(S, \psi, \hat{n}\right) \tag{7}$$

where $\Delta\psi$ = variation of soil suction, ψ; ΔS = variation of the degree of saturation of water corresponding to $\Delta\psi$ (e.g., from Point E to Point F); $\hat{n}$ = direction of the hydraulic path, which is equal to either −1 (for wetting) or 1 (for drying); and $K_p\left(S, \psi, \hat{n}\right)$ = slope of the scanning curve, which is written as

$$K_p\left(S, \psi, \hat{n}\right) = \overline{K}_p(S, \psi, \hat{n}) + d\left|\psi - \bar{\psi}(S, \hat{n})\right| / \times\left[r - \left|\psi - \bar{\psi}(S, \hat{n})\right|\right] \tag{8}$$

where d = fit parameter used to describe the scanning curve and can be determined using a measured first-order scanning curve or a point on a scanning curve; $\bar{\psi}\left(S, \hat{n}\right)$ = one of the boundary curves of the hysteretic loop [either the main drying curve (MDC), or the MWC]; and $\overline{K}_p\left(S, \hat{n}\right)$ = slope of the boundary curve (the MDC or the MWC). The differences in soil suction between Points M and N, $r(S)$, is the difference of suction between the MDC and MWC at the degree of saturation, S, as seen in Fig. 1(b).

With the procedure presented, the capillary hysteresis was described completely in the model. At this point in the process, the problem involved the specification of the two boundary curves (C′–D′ and D′–C′) of the hysteretic loop under the effect of air entrapment. To construct the model, the concept of the current maximum suction (denoted as $\psi_i^{\max}$) was introduced to define the maximum suction that a soil experiences during a continual drying process, as seen in Fig. 1(a). A unique, trapped saturation at zero soil suction (denoted as S_i^{trap}) for a specified $\psi_i^{\max}$ is

$$S_i^{\text{trap}} = S_{\max}^{\text{trap}}(1 - S_{ei}) \tag{9}$$

where S_{ei} = effective degree of saturation at $\psi_i^{\max}$ (Point D′ on the IDC), which is $S_{ei} = (S_i - S_r)/(1 - S_r)$, where S_i = degree of saturation at $\psi_i^{\max}$ on the IDC and S_r = residual degree of saturation of water; and S_i^{trap} and $S_{\max}^{\text{trap}}$ = current degree of saturation and the maximum degree of saturation of the trapped air, respectively [Fig. 1(a)]. A constraint is

$$S_i^{\text{trap}} = 1.0 - S_{i0} \tag{10}$$

It is important that the current maximum suction, $\psi_i^{\max}$ is replaced when the suction becomes greater than $\psi_i^{\max}$ as the soil dries. Correspondingly, S_{i0} is updated by the current $\psi_i^{\max}$ through Eqs. (9) and (10).

Once Point D′ was specified, Point C′ was determined using the method described in this subsection. Then, the wetting curve (D′–C′) and the drying curve (C′–D′) were determined by translating the parallel curves D–C and C–D, respectively [Fig. 1(a)].

The Chen et al. (2015) model had eight parameters (θ_s^d, θ_s^w, θ_r, α^d, α^w, n^d, n^w, and d) for the hysteretic SWRC. It had seven parameters for the boundary curves and only one parameter for the scanning curves. It had seven parameters (θ_s^d, θ_r, α^d, α^w, n^d, n^w, and d) for the effect of the capillary hysteresis only. The parameters θ_s^d, θ_r, α^d, and n^d were obtained by fitting the measured IDC using Eq. (1). The parameters θ_s^w, α^w, and n^w were obtained by fitting the measured MWC using Eq. (2). The parameter d was determined by validating the one measured point or curve included in the IDC and MWC loop using Eq. (7).

Numerical Model

A coupled seepage and deformation model for two-phase flow problems was developed by Chen and Wei (2016). The simulated framework is introduced in brief herein. The governing equations for the three-phase mixture system (solid, water, and air) are also presented in this section.

The linear momentum balance equations of water and air are given by

$$\eta^f \rho^f D^f \mathbf{v}^f / Dt - \eta^f \rho^f \mathbf{g} + \eta^f \nabla p^f = -\left(\eta^f\right)^2 \mu_f / \left(K_{\text{sat}} k_r^f\right)\left(\mathbf{v}^f - \mathbf{v}^s\right) \tag{11}$$

where D^f/Dt = the material derivative; η^f = volume fraction of the fluids (water and air); $p^f = p^w$ or pa on behalf of water and air pressure, respectively; $\mathbf{g}$ is the gravity acceleration or the centrifugal acceleration in a centrifuge test; $\mathbf{v}^f = \mathbf{v}^w$ or $\mathbf{v}^a$ on behalf of velocity of the water or air, respectively; $\mathbf{v}^s$ = velocity of the solid matrix, which is equal to $\dot{\mathbf{u}}^s$, where $\mathbf{u}^s$ is the deformation vector of the solid matrix; K_{sat} = intrinsic permeability coefficient of the water phase; and μ_f = dynamic viscosity of the fluids. The terms μ_w and μ_a refer to the dynamic viscosity for water and air, respectively. The saturated permeability coefficient of water can be determined by $k_{\text{sat}} = K_{\text{sat}}\rho g/\mu_w$. The term k_r^f is the relative hydraulic conductivity function, which was proposed by Mualem (1976) as follows:

$$k_r^w = (S_e)^{0.5}\left[1 - \left(1 - S_e^{1/m}\right)^m\right]^2 \tag{12a}$$

$$k_r^a = (1 - S_e)^{0.5}\left(1 - S_e^{1/m}\right)^{2m} \tag{12b}$$

where k_r^w and k_r^a = relative permeability coefficient of the water and air, respectively; and m = empirical parameter.

The equilibrium equation for the mixture is given as follows:

$$\rho D^s \mathbf{v}^s / Dt = \nabla \cdot \boldsymbol{\sigma} + \rho \mathbf{g} \tag{13}$$

where $\boldsymbol{\sigma}$ = total stress tensor; and ρ = total density of the mixture.

The mass balance equation of the pore water and air is

$$\eta_0\left(D^s S^f / Dt\right) + \left(\eta_0 S^f / K_f\right)\left(D^s \rho^f / Dt\right) + \nabla \cdot \mathbf{q}^f + S^f \nabla \cdot \mathbf{v}^f = 0 \tag{14}$$

where $\mathbf{q}^f = \mathbf{q}^w$ or $\mathbf{q}^a$, on behalf of permeability velocity of the pore water and air, respectively, in which $\mathbf{q}^w = \eta S(\mathbf{v}^f - \mathbf{v}^s)$ and

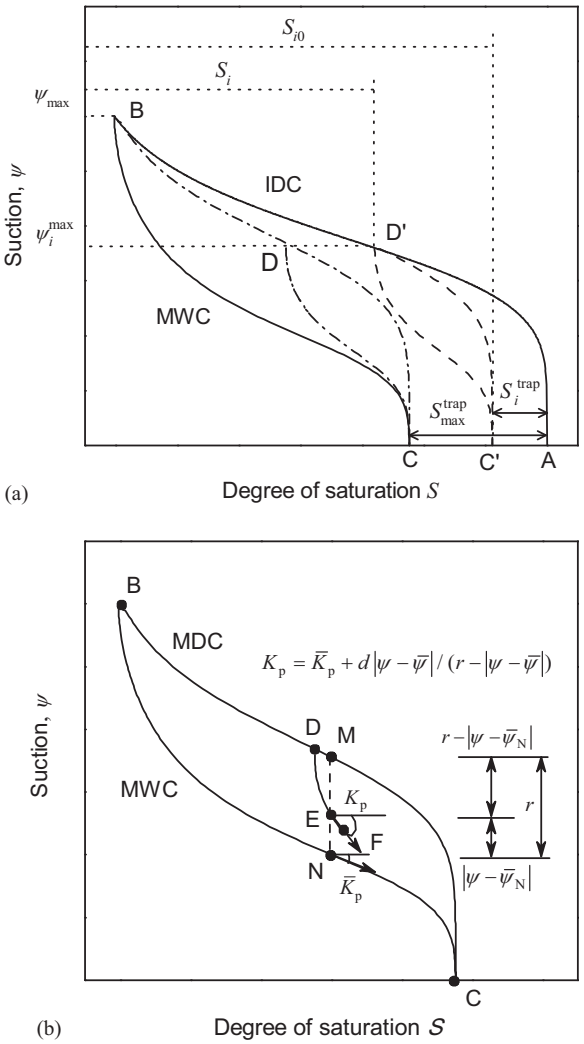

Fig. 1. (a) Hydraulic hysteresis model and (b) determination of the scanning curve in the closed loop.

$\mathbf{q}^a = \eta(1-S)\times(\mathbf{v}^f - \mathbf{v}^s)$; and η and η_0 = porosity and initial porosity, respectively.

Eqs. (11), (13), and (14) include five independent equations and seven unknown variables: $\mathbf{u}^s$, $\mathbf{q}^w$, $\mathbf{q}^a$, $\boldsymbol{\sigma}$, p^w, p^a, and S. Hence, two additional constitutive equations were needed to be introduced to obtain a closure solution for two-phase flow problems, which include the stress-strain and SWRC relations [e.g., Khalili et al. (2008); Song and Borja (2014)]. The SWRC equation is given in Eq. (7) to describe the variation of water content and matric suction under the effect of hydraulic hysteresis. The solid skeleton of soil was assumed to be isotropic and linearly elastic. The stress-strain relation is determined by the following incremental form:

$$d\boldsymbol{\sigma}' = \mathbf{D}_T : d\boldsymbol{\varepsilon} \tag{15}$$

where $\boldsymbol{\sigma}'$ = effective stress tensor; $\boldsymbol{\varepsilon}$ = infinitesimal strain tensor; and $\mathbf{D}_T$ = tangent modulus, where $\mathbf{D}_T = (K - 2/3G)\mathbf{1}\otimes\mathbf{1} + 2G\mathbf{I}$, $\mathbf{I}$ is the fourth-order unit isotropic tensor, and K and G are the rigid modulus and shear modulus of the solid skeleton, respectively. The effective stress (Lu et al. 2010) is expressed as follows:

$$\boldsymbol{\sigma}' = \boldsymbol{\sigma} - p^a\mathbf{1} + S_e(p^a - p^w)\mathbf{1} \tag{16}$$

where $\mathbf{1}$ = second-order unit isotropic tensor; and ψ = soil suction equal to $(p^a - p^w)$. The basic variables, including deformation, $\mathbf{u}^s$, and water pressure, p^w, and air pressure, p^a, defined in the problem, were solved by introducing Eqs. (7) and (15), which are complementary equations.

The governing Eqs. (11), (13), and (14) can be discrete in the space and time scales according to the standard Galerkin method given the initial and boundary conditions. A simple matrix equation describing the seepage and deformation process for two-phase flow problems is given as follows:

$$\mathbf{c}\dot{\mathbf{U}} + \boldsymbol{\kappa}\mathbf{U} = \mathbf{f} \tag{17}$$

where $\mathbf{U}$ = array of the node variables, which includes the unknown deformation, $\mathbf{u}^s$, and water pressure, p^w, and air pressure p^a, of the nodes; $\mathbf{c}$ and $\boldsymbol{\kappa}$ = coefficient matrices; and $\mathbf{f}$ = generalized force. Chen and Wei (2016) gave the details of $\mathbf{c}$, $\boldsymbol{\kappa}$, and $\mathbf{f}$. Because of the initial conditions, the values of u^s, p^w, and p^a of each node were obtained by solving Eq. (17) through the numerical iteration implemented in the FEM.

Model Assessments

The SWRC model with the effect of hydraulic hysteresis developed by Chen et al. (2015) was included in the numerical model for describing two-phase flow problems under drying and wetting conditions. Then, the numerical model was implemented into the program code U-DYSAC (Muraleetharan and Wei 2001); the program was used to analyze two-phase flow problems under quasi-static conditions. The Kool and Parker (1987) model was implemented with the software HYDRUS (Šimůnek et al. 2012). Thus, HYDRUS was used to simulate the same one-dimension (1D) unsaturated flow problems. Moreover, to verify the importance of hydraulic hysteresis, the IDC was also used in the numerical model to simulate the same flow problems for which the hydraulic hysteresis was ignored. Two different unsaturated flow examples were used to assess the validity of the two hysteresis models by comparing the predicted curves with measured data.

Comparison of Two Numerical Codes

Before assessing the validity of the two SWRC constitutive models developed by Kool and Parker (1987) and Chen et al. (2015), the difference between the two numerical frameworks (U-DYSAC and HYDRUS) for solving the unsaturated flow problem needed to be explored. To this end, a sand column test was adopted to test the two numerical codes. The detailed information for the test and measured hydraulic–mechanical parameters were presented by Gillham et al. (1976, 1979). In this section, the difference between the two numerical frameworks for simulating the unsaturated flow problem is the main concern. Therefore, the IDC was used in the models only to simulate the unsaturated flow, and the effect of hydraulic hysteresis was not considered. The height of the sand column was 60 cm. At the initial stage, the sand column was fully saturated along the entire sand column. The boundary conditions were as follows: (1) at the top, the value of q_z was 0.0; (2) for the base, the change of the pressure head was from 60 to 0 cm; and (3) the two sides were impermeable to water and permeable to air. The water was discharged from the base of the sand column when the water pressure deceased gradually. The material and model parameters used in the HYDRUS and U-DYSAC models are listed in Table 1.

The simulated results and measured data are shown in Figs. 2(a and b). The water pressure heads at three different depths decreased gradually when the boundary pressure decreased at the

Table 1. Material properties and SWRC parameters for the Fontainebleau and dune sands

Parameter	Fontainebleau sand	Dune sand
Saturated hydraulic conductivity [k_{sat} (m/s)]	7.22×10^{-5}	7.67×10^{-5}
Density of solid phase [ρ^s (kg/m^3)]	2.65×10^3	2.65×10^3
Density of water [ρ^w (kg/m^3)]	1.00×10^3	1.00×10^3
Density of air [ρ^a (kg/m^3)]	1.20	1.20
Gravity [g (m/s^2)]	9.81	9.81
Dynamic fluid viscosity of water [μ_w (Pa s)]	1.00×10^{-3}	1.00×10^{-3}
Dynamic fluid viscosity of air [μ_a (Pa s)]	1.80×10^{-5}	1.80×10^{-5}
Porosity [η_0 (cm^3/cm^3)]	0.340	0.301
Residual volumetric water content [θ_r (cm^3/cm^3)]	0.040	0.095
Saturated volumetric water content [θ_s (cm^3/cm^3)]	0.340	0.301
For IDC (n^d)	7.93	8.40
For IDC [α^d (cm^{-1})]	0.026	0.029
For MWC (n^w)	4.22	5.57
For MWC [α^w (cm^{-1})]	0.05	0.049
Scanning parameter [d (cm)]	100	400

bottom of the column. Fig. 2(a) shows that the simulated water pressure heads from the two numerical codes at three different depths coincided very well. Similarly, the agreement was quite good between the predicted water content from the two numerical codes at three depths. Hence, the difference of the two finite-element codes could be ignored when solving the unsaturated flow problems when the effect of airflow was not significant.

Assessment of the Two Hysteresis Models

The first experiment was done in a sand column of 1-m height under variable flux conditions (Hoa et al. 1977) as shown in Fig. 3(a). Tensiometers and the gamma ray absorption method were used to measure the soil suction and water content, respectively. The material used in the experiment was Fontainebleau sand. The physical properties of the sand are listed in Table 1. The sand column was fully saturated before the experiment started. The boundary conditions were specified as follows: (1) for the top, the flux, q_z, was 0.0 cm/h and the air pressure, p^a, was 101.3 kPa; (2) for the two sides, q_x, was 0.0 cm/h, p^a was 101.3 kPa, and u_x was 0 cm; and (3) for the base, $u_x = u_z = 0$ cm, p^a was 101.3 kPa, and $q_z = q(t)$ cm/h [Fig. 3(b)]. In this paper, *cm* for the flux unit means cm/cm^2. The comparison of the modeling results and measured data at the two profiles, of height 60 and 80 cm, is shown in Fig. 4. The model parameters for the Kool and Parker (1987) and Chen et al. (2015) models are listed in Table 1.

The measured data presented in Fig. 4 show that the sandy soil in the column experienced the drying, wetting, and redrying processes at the two different heights: 60 and 80 cm. The comparison of the two models for the measured soil suction to the predicted curves is presented in Fig. 4(a). The results show that the curves predicted by the Chen et al. (2015) model best matched the measured suction under the wetting and redrying processes, especially at the height of 60 cm. At the height of 80 cm, the predicted curves from the Kool and Parker (1987) model were similar to the ones from the model ignoring the hysteretic effect (the IDC). However, the predicted curves from the Kool and Parker (1987) model and the IDC model both deviated from the measured data under the subsequent wetting

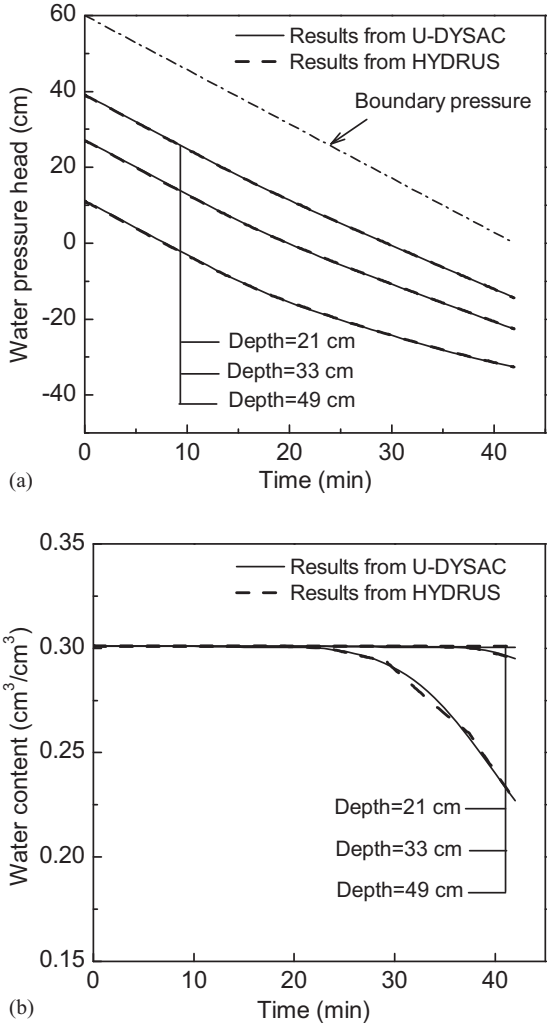

Fig. 2. Comparison of the predicted curves from U-DYSAC2 and HYDRUS 1D: (a) water pressure head; (b) water content.

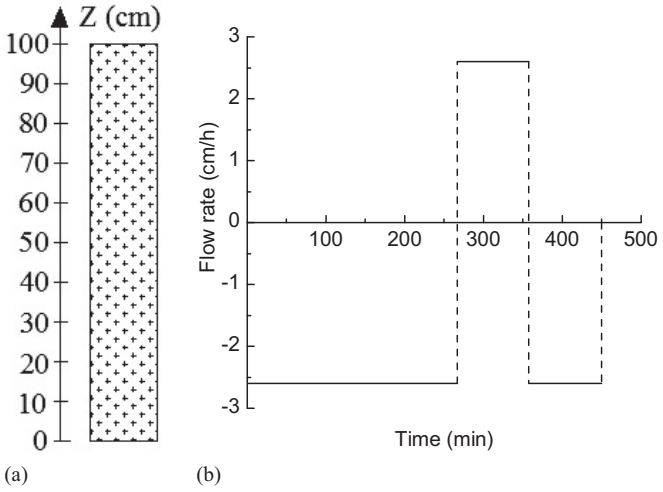

Fig. 3. (a) Fontainebleau sand column and (b) variations of the flow rates at the bottom of the column.

and redrying processes. A similar tendency was also observed in Fig. 4(b) for the evolution of water content. The consistency of the simulated results using the Chen et al. (2015) model and the

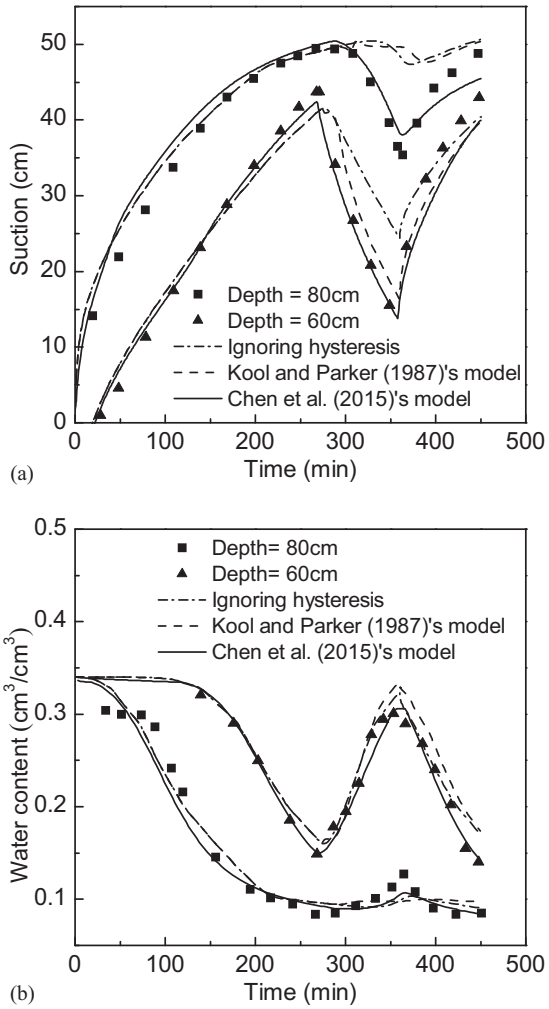

Fig. 4. Comparison of the measured data and predicted curves for the Fontainebleau sand using the two SWRC models: (a) suction; (b) water content.

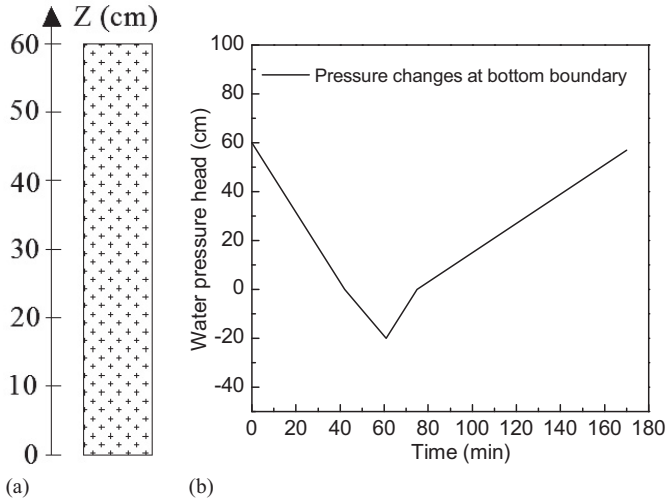

Fig. 5. (a) Dune sand column and (b) variations of water pressure heads at the bottom of the column.

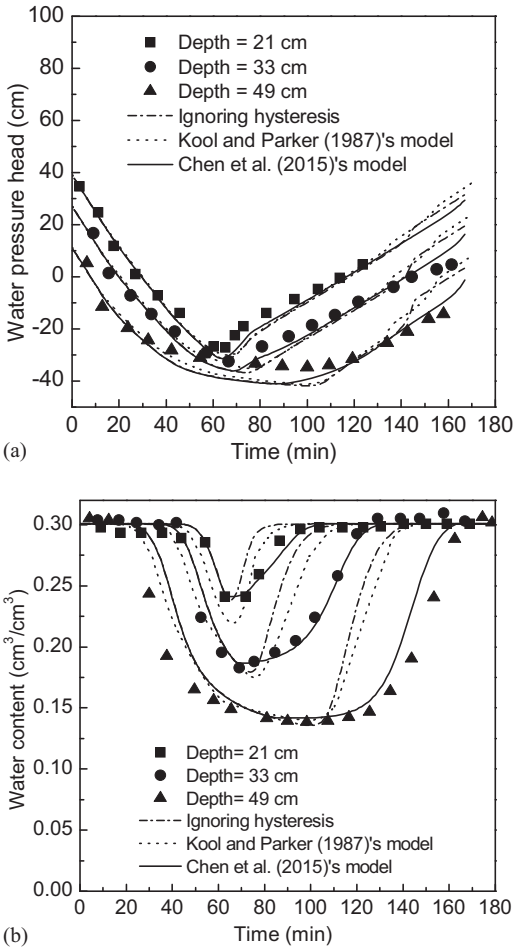

Fig. 6. Comparison of the measured data and predicted curves for the dune sand using the two SWRC models: (a) water pressure head; (b) water content.

measured data is shown in Fig. 4(b). According to Fig. 4, the predicted curves from ignoring hysteresis and the Kool and Parker (1987) model both failed to capture the change of the pressure head and water content at two different depths under wetting and redrying conditions. Although one additional parameter was used to describe the scanning curves in the Chen et al. (2015) model, the capacity for capturing the hydraulic hysteresis was quite reliable and robust.

Another experiment was performed by Gillham et al. (1979) on packed dune sand column with a height of 60 cm, as presented in Fig. 5(a). A porous PVC barrier was set at the bottom of the column to prevent the sand flow and give passage to the water. The air vents at the two sides were opened along the soil column to hold the atmospheric pressure condition in the entire soil system. Fig. 5(b) shows that a variation of the water pressure head was applied to the bottom of the column. The water pressure heads were determined by a tensiometer transducer, and the gamma ray attenuation method was used to measure the water content in the sandy soil. The measured SWRC was presented in Gillham et al. (1976). The material properties of the dune sand are listed in Table 1.

The sand column was initially at a fully saturated state. The boundary conditions of the experiment are given as follows: (1) for the top, q_z was 0.0 and p^a was 101.3 kPa; (2) for the two sides, q_x was 0.0 cm/h, p^a was 101.3 kPa, and u_x was 0 cm; and (3) at the bottom, $u_x = u_z = 0$ cm, p^a was 101.3 kPa, and $p = p(t)$ as shown in Fig. 4(a). The Kool and Parker (1987) and Chen et al. (2015) models

were both used to simulate the same seepage problem, and the predicted curves and measured data are both presented in Fig. 6. The material and model parameters used in the simulation are listed in Table 1.

The measured drying and wetting data of the dune sand at different heights in the column are shown in Fig. 6 under variations of the water pressure head. Figs. 6(a and b) show the predicted and measured variations of the water content and water pressure head at three different depths. Compared to the measured data, the results from the Chen et al. (2015) model showed the best predictivity for both the water pressure head and water content. In particular, the predicted change of the water content by the Chen et al. (2015) model agreed much better with the experimental data than did that from the IDC and Kool and Parker (1987) models [Fig. 6(b)]. Although the predicted curves from the Kool and Parker (1987) model were better than the ones from the IDC model (ignoring hysteresis), the predicted water content from the two models both deviated significantly from the measured data during the wetting process. The comparisons show that the Chen et al. (2015) model described hydraulic hysteresis behavior much more accurately in unsaturated flow than the others. Moreover, the results show that the effect of hydraulic hysteresis played a significant role in the unsaturated flow process under drying and wetting conditions.

Conclusions

This paper presented the description of a numerical FEM used to simulate unsaturated flow problems under wetting and drying conditions. A new SWRC model was introduced with a numerical code, through which the effect of hydraulic hysteresis was addressed. One additional parameter was used to describe the scanning curves. By comparing the measured data to the predicted curves, the proposed model was validated using the measured hysteretic data under varied flux and pressure boundary conditions.

To show the reliability of the hysteresis models, HYDRUS included the Kool and Parker (1987) model was used to solve the same unsaturated flow problems. By comparing the results from two hysteretic SWRC models, the results showed that the predicted curves by the Chen et al. (2015) model were much closer to the measured data in both experiments. The Chen et al. (2015) model showed excellent performance in describing the effect of hydraulic hysteresis in unsaturated flow. Furthermore, the results also showed that water pressure and water content deviated greatly from the measured data when the effect of hydraulic hysteresis was ignored. Hence, it is crucial to properly address the effect of hydraulic hysteresis in simulating unsaturated flow problems.

Acknowledgments

This research was supported by the National Natural Science Foundation of China (Grants 41472286 and 41572293).

References

Baum, R. L., J. W. Godt, and W. Z. Savage. 2010. "Estimating the timing and location of shallow rainfall-induced landslides using a model for transient, unsaturated infiltration." *J. Geophys. Res.* 115: 1–26. https://doi.org/10.1029/2009JF001321.

BeVille, S. H., B. B. Mirus, B. A. Ebel, G. G. Mader, and K. Loague. 2010. "Using simulated hydrologic response to revisit the 1973 Lerida Court landslide." *Environ. Earth Sci.* 61 (6): 1249–1257. https://doi.org/10.1007/s12665-010-0448-z.

Bond, W. J., and N. Collis-George. 1981. "Ponded infiltration into simple soil systems: 1. The saturation and transition zones in the moisture content profiles." *Soil Sci.* 131 (4): 202–209. https://doi.org/10.1097/00010694-198104000-00002.

Chen, P., B. Mirus, N. Lu, and J. W. Godt. 2017. "Effect of hydraulic hysteresis on stability of infinite slopes under steady infiltration." *J. Geotech. Geoenviron. Eng.* 143 (9): 04017041. https://doi.org/10.1061/(ASCE)GT.1943-5606.0001724.

Chen, P., and C. Wei. 2016. "Numerical procedure for simulating the two-phase flow in unsaturated soils with hydraulic hysteresis." *Int. J. Geomech.* 16 (1): 04015030. https://doi.org/10.1061/(ASCE)GM.1943-5622.0000505.

Chen, P., C. Wei, J. Liu, and T. Ma. 2013. "Strength theory model of unsaturated soils with suction stress concept." *J. Appl. Math.* 2013: 1–11. https://doi.org/10.1155/2013/756854.

Chen, P., C. Wei, and T. Ma. 2015. "Analytical model of soil-water characteristics considering the effect of air entrapment." *Int. J. Geomech.* 15 (6): 04014102. https://doi.org/10.1061/(ASCE)GM.1943-5622.0000462.

Ebel, B. A., K. Loague, and R. I. Borja. 2010. "The impacts of hysteresis on variably saturated hydrologic response and slope failure." *Environ. Earth Sci.* 61 (6): 1215–1225. https://doi.org/10.1007/s12665-009-0445-2.

Feng, M., and D. G. Fredlund. 1999. "Hysteretic influence associated with thermal conductivity sensor measurements." In *52nd Canadian Geotechnical Conf.*, 651–657. Richmond, BC, Canada: Canadian Geotechnical Society.

Gillham, R. W., A. Klute, and D. F. Heermann. 1976. "Hydraulic properties of a porous medium measurement and empirical representation." *Soil Sci. Soc. Am. J. Abstr.* 40 (2): 203–207. https://doi.org/10.2136/sssaj1976.03615995004000020008x.

Gillham, R. W., A. Klute, and D. F. Heermann. 1979. "Measurement and numerical simulation of hysteretic flow in a heterogeneous porous medium." *Soil Sci. Soc. Am. J. Abstr.* 43 (6): 1061–1067. https://doi.org/10.2136/sssaj1979.03615995004300060001x.

Hoa, N. T., R. Gaudu, and C. Thirriot. 1977. "Influence of hysteresis effect on transient flows in saturated-unsaturated porous-media." *Water Resour. Res.* 13 (6), 992–996. https://doi.org/10.1029/WR013i006p00992.

Huang, H.-C., Y.-C. Tan, C.-W. Liu, and C.-H. Chen. 2005. "A novel hysteresis model in unsaturated soil." *Hydrol. Processes* 19 (8): 1653–1665. https://doi.org/10.1002/hyp.5594.

Kechavarzi, C., K. Soga, and T. H. Illangasekare. 2005. "Two-dimensional laboratory simulation of LNAPL infiltration and redistribution in the vadose zone." *J. Contam. Hydrol.* 76 (Feb): 211–233. https://doi.org/10.1016/j.jconhyd.2004.09.001.

Khalili, N., M. A. Habte, and S. Zargarbashi. 2008. "A fully coupled flow deformation model for cyclic analysis of unsaturated soils including hydraulic and mechanical hystereses." *Comput. Geotech.* 35 (6): 872–889. https://doi.org/10.1016/j.compgeo.2008.08.003.

Khoury, N., R. Brooks, C. Khoury, and D. Yada. 2012. "Modeling resilient modulus hysteretic behavior with moisture variation." *Int. J. Geomech.* 12 (5): 519–527. https://doi.org/10.1061/(ASCE)GM.1943-5622.0000140.

Khoury, C. N., and G. A. Miller. 2012. "Influence of hydraulic hysteresis on the shear strength of unsaturated soils and interfaces." *Geotech. Test. J.* 35 (1): 135–149. https://doi.org/10.1520/GTJ103616.

Kool, J. B., and J. C. Parker. 1987. "Development and evaluation of closed-form expressions for hysteretic soil hydraulic properties." *Water Resour. Res.* 23 (1): 105–114. https://doi.org/10.1029/WR023i001p00105.

Li, Y., P. Wu, Z. Xia, Q. Yang, G. Flores, H. Jiang, M. Kamon, and B. Yu. 2014. "Changes in residual air saturation after thorough drainage processes in an air-water fine sandy medium." *J. Hydrol.* 519: 271–283. https://doi.org/10.1016/j.jhydrol.2014.07.019.

Likos, W. J., N. Lu, and J. W. Godt. 2014. "Hysteresis and uncertainty in soil water-retention curve parameters." *J. Geotech. Geoenviron. Eng.* 140 (4): 04013050. https://doi.org/10.1061/(ASCE)GT.1943-5606.0001071.

Liu, C., and K. Muraleetharan. 2012. "Coupled hydro-mechanical elastoplastic constitutive model for unsaturated sands and silts. I: Formulation." *Int. J. Geomech.* 12 (3): 239–247. https://doi.org/10.1061/(ASCE)GM.1943-5622.0000146.

Lu, N., J. W. Godt, and D. T. Wu. 2010. "A closed-form equation for effective stress in unsaturated soil." *Water Resour. Res.* 46 (5): W05515. https://doi.org/10.1029/2009WR008646.

Lu, N., M. Kaya, B. D. Collins, and J. W. Godt. 2013. "Hysteresis of unsaturated hydromechanical properties of a silty soil." *J. Geotech. Geoenviron. Eng.* 139 (3): 507–510. https://doi.org/10.1061/(ASCE)GT.1943-5606.0000786.

Ma, T., C. Wei, H. Wei, and W. Li. 2016. "Hydraulic and mechanical behavior of unsaturated silt: Experimental and theoretical characterization." *Int. J. Geomech.* 16 (6): D4015007. https://doi.org/10.1061/(ASCE)GM.1943-5622.0000576.

Mualem, Y. 1976. "A new model for predicting hydraulic conductivity of unsaturated porous-media." *Water Resour. Res*, 12 (3): 513–522. https://doi.org/10.1029/WR012i003p00513.

Mualem, Y., and G. Dagan. 1975. "A dependent domain model of capillary hysteresis." *Water Resour. Res.* 11 (3): 452–460. https://doi.org/10.1029/WR011i003p00452.

Muraleetharan, K., and C. Wei. 2001. "U-DYSAC2: Dynamic unsaturated soil analysis code for 2-dimensional problems." Technical Rep. Norman, OK: School of Civil Engineering and Environmental Science, Univ. of Oklahoma.

Parker, J. C., and R. J. Lenhard. 1987. "A model for hysteretic constitutive relations governing multiphase flow: 1. saturation-pressure relations." *Water Resour Res.* 23 (12): 2187–2196. https://doi.org/10.1029/WR023i012p02187.

Parlange, J.-Y. 1976. "Capillary hysteresis and relationship between drying and wetting curve." *Water Resour. Res.* 12 (2): 224–228. https://doi.org/10.1029/WR012i002p00224.

Pasha, A. Y., A. Khoshghalb, and N. Khalili. 2017. "Hysteretic model for the evolution of water retention curve with void ratio." *J. Eng. Mech.* 143 (7): 04017030. https://doi.org/10.1061/(ASCE)EM.1943-7889.0001238.

Pham, H. Q., D. G. Fredlund, and S. L. Barbour. 2005. "A study of hysteresis models for soil-water characteristic curves." *Can. Geotech. J.* 42 (6): 1548–1568. https://doi.org/10.1139/t05-071.

Pickens, J. F., and R. W. Gillham. 1980. "Finite element analysis of solute transport under hysteretic unsaturated flow conditions." *Water Resour. Res.* 16 (6): 1071–1078. https://doi.org/10.1029/WR016i006p01071.

Poulovassilis, A. 1970. "The effect of the entrapped air on the hysteresis curves of a porous body and on its hydraulic conductivity." *Soil Sci.* 109 (3): 154–162. https://doi.org/10.1097/00010694-197003000-00003.

Poulovassilis, A., and E. C. Childs. 1971. "The hysteresis of pore water: the non-independence of domains." *Soil Sci.* 112 (5): 301–312. https://doi.org/10.1097/00010694-197111000-00002.

Scott, P. S., G. J. Farquhar, and N. Kouwen. 1983. "Hysteresis effects on net infiltration." In *Proc., National Conference on Advances in Infiltration*, 163–170. St. Joseph, MI: American Society of Agricultural and Biological Engineers.

Seymour, R. M. 2000. "Air entrapment and consolidation occurring with saturated hydraulic conductivity changes with intermittent wetting." *Irrig. Sci.* 20 (1): 9–14. https://doi.org/10.1007/PL00006716.

Sheng, D., and A.-N. Zhou. 2011. "Coupling hydraulic with mechanical models for unsaturated soils." *Can. Geotech. J.* 48 (5): 826–840. https://doi.org/10.1139/t10-109.

Šimůnek, J., M. Th. van Genuchten, and M. Šejna. 2012. *The HYDRUS software package for simulating two- and three-dimensional movement of water, heat, and multiple solutes in variably-saturated media, version 2.0.* Prague, Czech Republic: PC Progress.

Song, X., and R. I. Borja. 2014. "Mathematical framework for unsaturated flow in the finite deformation range." *Int. J. Numer. Methods Eng.* 97 (9): 658–682. https://doi.org/10.1002/nme.4605.

Stonestrom, D. A., and J. Rubin. 1989. "Water-content dependence of trapped air in two soils." *Water Resour. Res.* 25 (9): 1947–1958. https://doi.org/10.1029/WR025i009p01947.

Sun, D., D. Sheng, and S. W. Sloan. 2007. "Elastoplastic modelling of hydraulic and stress–strain behaviour of unsaturated soils." *Mech. Mater.* 39 (3): 212–221. https://doi.org/10.1016/j.mechmat.2006.05.002.

Sun, D., W. Sun, and X. Li. 2010. "Effect of degree of saturation on mechanical behaviour of unsaturated soils and its elastoplastic simulation." *Comput. Geotech.* 37 (5): 678–688. https://doi.org/10.1016/j.compgeo.2010.04.006.

Sun, D. M., Y. G. Zang, P. F. Feng, and S. Semprich. 2016. "Quasi-saturated zones induced by rainfall infiltration." *Transp. Porous Media* 112 (1): 77–104. https://doi.org/10.1007/s11242-016-0633-y.

Tami, D., H. Rahardjo, and E.-C. Leong. 2004. "Effects of hysteresis on steady-state infiltration in unsaturated Slopes." *J. Geotech. Geoenviron.* 130 (9): 956–967. https://doi.org/10.1061/(ASCE)1090-0241(2004)130:9(956).

Vachaud, G., and J.-L. Thony. 1971. "Hysteresis during infiltration and redistribution in a soil column at different initial water contents." *Water Resour. Res.* 7 (1): 111–127. https://doi.org/10.1029/WR007i001p00111.

van Genuchten, M. Th. 1980. "A closed-form equation for predicting the hydraulic conductivity of unsaturated soils." *Soil Sci. Soc. Am. J.* 44 (5): 892–898. https://doi.org/10.2136/sssaj1980.03615995004400050002x.

Wei, C., and M. M. Dewoolkar. 2006. "Formulation of capillary hysteresis with internal state variables." *Water Resour. Res.* 42 (7): W07405. https://doi.org/10.1029/2005WR004594.

Wheeler, S. J., R. S. Sharma, and M. S. R. Buisson. 2003. "Coupling of hydraulic hysteresis and stress- strain behaviour in unsaturated soils." *Géotechnique* 53 (1): 41–54. https://doi.org/10.1680/geot.2003.53.1.41.

Yang, C., D. Sheng, and J. P. Carter. 2012. "Effect of hydraulic hysteresis on seepage analysis for unsaturated soils." *Comput. Geotech.* 41 (Apr): 36–56. https://doi.org/10.1016/j.compgeo.2011.11.006.